

# CFD Study of the Fluid Viscosity Variation and Effect on the Flow in a Stirred Tank

Achouri Ryma, Hatem Dhaouadi, Hatem Mhiri, Philippe Bournot

**Abstract**—Stirred tanks are widely used in all industrial sectors. The need for further studies of the mixing operation and its different aspects comes from the diversity of agitation tools and implemented geometries in addition to the specific characteristics of each application. Viscous fluids are often encountered in industry and they represent the majority of treated cases, as in the polymer sector, food processing, pharmaceuticals and cosmetics. That's why in this paper, we will present a three-dimensional numerical study using the software Fluent, to study the effect of varying the fluid viscosity in a stirred tank with a Rushton turbine. This viscosity variation was performed by adding carboxymethylcellulose (CMC) to the fluid (water) in the vessel. In this work, we studied first the flow generated in the tank with a Rushton turbine. Second, we studied the effect of the fluid viscosity variation on the thermodynamic quantities defining the flow. For this, three viscosities (0.9% CMC, 1.1% CMC and 1.7% CMC) were considered.

**Keywords**—CFD, CMC, Mixing, Viscosity, Rushton turbine.

## I. INTRODUCTION

FROM the coffee cup to the giant cement silo, a mixing science was developed to study all interactions that can take place inside it: heat transfer, mass transfer, the mixer power, the viscosity and shear... Today, industries such as pharmaceuticals, food industry or water treatment have become aware of the need for a serious consideration of mixing as the mixture sit for a long time on empirical correlations. Our research was made to give a numerical study of a stirred tank with a Rushton turbine, and to try to improve the mixing performances when changing the fluid viscosity. This improvement is made by changing the turbine position into the tank, and to study the hydrodynamic parameters of each position. Some research focused on the geometrical parameter of the tank like [1] and the applications of CFD method in a large scale tank [2]. The case of tanks with and without internals obstructions was also studied [3], using in his work experiments and CFD Models. Many CFD approaches for studying and predicting the flow field in a stirred tank were studied: A comparison was made between several CFD approaches [4] for predicting the flow field in a mixed reactor.

Ryma Achouri and Hatem Mhiri are with the UTTPI, National Engineering School of Monastir, Tunisia (phone: 0021625387105; fax: (+216) 73 50 05 14; e-mail: ryma\_achouri@yahoo.fr; hatem.mhiri@enim.rnu.tn).

Hatem Dhaouadi is with University of Monastir, Sciences University, UR1204- Applied Chemistry Environment (e-mail: hatem.dhaouadi@fsm.rnu.tn).

Philippe Bournot is with IUSTI, UMR CNRS 6595, 5 rue Enrico Fermi, Technopole de Château-Gombert, 1303 Marseille, France (e-mail: bournot@univmed.fr).

Some used the code Fluent [5] to simulate the laminar and turbulent flow generated by a Rushton turbine in a baffled tank. They proposed and applied numerical simulation by Snapshot (method of the black box) and has validated his results by his previous experimental work. The sliding mesh was assessed [6] by CFD and measured by LDA the flow present in a vessel with four baffles and agitated by a Rushton turbine. A study [7] focused on the energy consumption of the flow in a stirred tank, for different types of agitation mobiles. A comparison of the parameters of the flow (speed, turbulent kinetic energy, energy dissipation rate ...), for the same energy, was conducted to characterize the flow generated by stirrers. The CFD predictions have been validated by LDA measurements. The available techniques for the study of flow induced by different types of agitators, such as classical techniques of measuring velocity by the pressure difference, the tube of Pitot and the hot wire, or even new as LDV, fluorescent techniques induced by laser and the PIV, were reviewed and discussed [8]. LES model was adapted [9] and the sliding mesh model to study a tank mixed by a Rushton turbine equipped with six blades. The results were assessed based on experimental studies [10] and showed that the LES model is a reliable tool to study the time-varying behavior of turbulent flow in agitated tanks. Other researchers [11] were interested by the Rushton turbine submergence effect on the velocity field. The results showed that for a small clearance, the fluid flow is changing from a radial (at two loops) typical field to an axial field similar to that generated by a propeller. They found that this profile leads to an increase of the axial flow and a reduction in the time of mixture for the same power number. Other ones [12] have compared three methods for the simulation of mixing in a baffled tank. Predictions of CFD were presented for the Rushton turbines and propeller and results were compared with the experience and literature. A different study [13] was about the distribution of the turbulent energy dissipation rate  $\epsilon$  in a tank agitated by a Rushton turbine by a CFD study based on sliding mesh technique. They showed that the estimations of  $\epsilon$  obtained from the macro scales of turbulence may overestimate the amount of energy dissipated in the volume swept by the turbine, while LDA studies indicate that a good amount of energy is dissipated around the walls and baffles. Concerning the studies on the effect of viscosity, some studies were experimental [14] using the LDV measurement to calculate the hydraulic efficiency and structure of turbulence for three agitators: Rushton turbine agitators and two axial flow agitators: a Mixel TT and Lightnin A310. Mixel TT had the best performance for a

viscous liquid (solution 1% CMC). All three had a relatively low efficiency. The authors found that the energy was mainly dissipated in the stream swept by the turbine and the main circulation loop. Other researchers added the numerical method [15] and have seen that the numerical simulation of viscous fluids in a stirred tank is insufficient and further development is required. They made the numerical simulation by CFD and PIV experimental study to examine the flow field of a viscous fluid in a tank agitated by a Rushton turbine with four blades. The studied solution is the mixture of water with different concentrations of glycerol. As a result, the mean velocity, turbulent energy, the pumping of fluids and the flow field change with the fluid viscosity. This numerical study was performed with the commercial code CFX4.4 and a sliding mesh. A recent study [16] attempted to generate the data flow of non-Newtonian fluids by conducting tracer experiments in a tank stirred by an anchor-type stirrer. The fluids studied are water, castor oil, methyl esters of castor oil, carboxymethylcellulose (solution 0.5 and 1% concentration), suspension of pulp (0.5% and 2 % concentration) and the suspension of starch (2% and 4% concentration) with the presence or absence of aeration. The authors found an increase in the efficiency of mixing with increasing rotational speed. The numerical fluid mechanics (CFD) is a robust tool in the prediction of flow in stirred tanks. The commercial code "Fluent" will be the CFD tool of this work which will focus on the modeling and on the numerical simulation of a stirred reactor with a Rushton turbine, including the fluid viscosity effect in such a system. This article presents our recent efforts for a better understanding of the turbulent flow in a stirred tank with a Rushton turbine, and for the visualization of the fluid viscosity effect. For the best description of the fluid flow, we used the Euler-Euler multiphase model and the turbulence model k-ε standard available in Fluent to describe the fluid flow in this type of turbine and also to study its performance, in order to optimize the stirring process and to improve the hydrodynamic parameters governing the fluid flow.

## II. CFD MODELING

### A. Studied Field

The studied field is a flat bottomed and an unbaffled tank, having a Rushton turbine with 6 blades as a mixer. The diameter of the tank,  $T$ , is equal to 0.36m, height  $H$  is equal to five quarts of  $T$  ( $H = 5/4T = 0.45\text{m}$ ), and the water level in the tank is  $h$  equal to three quarts of  $T$  ( $h = 3/4T = 0.27\text{m}$ ). The clearance (distance between the bottom of the tank and the turbine) of our turbine is  $C = 0.2\text{m}$ . The geometry of our field is represented in Fig. 1, and the dimensions of the Rushton turbine are resumed in Table I.

TABLE I

DIMENSIONS OF THE RUSHTON TURBINE		
Designation	Variable	Value (m)
$D$	Impeller Diameter	0.1243
$d$	Turbine's disk diameter	0.0843
$E$	Thickness of the turbine's disk	0.002
$L_p$	Blade Length	0.025
$l_p$	Blade width	0.02
$e_p$	Blade thickness	0.002

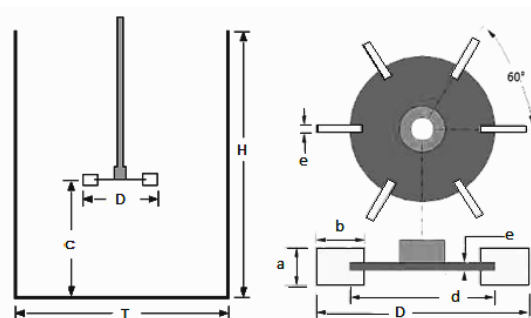


Fig. 1 Dimensions of the studied field

### B. Mesh and Boundary Conditions

The mesh creation is a delicate stage. Mesh quality is defined by the refinement of the mesh. In fact a fairly tight mesh leads to more accurate results while it increases significantly the number of meshes resulting in a longer computation time. It is necessary to define an area surrounding the turbine rotor (MRF: Moving Reference Frame) and a stator area. For an optimal mesh we worked in two steps: The first step is to divide the area into three parts. The middle area, which contains the Rushton type turbine, has a tighter mesh than the two others. It includes the MRF, with a tetrahedral mesh and the free surface with a mesh size even more refined for a better accuracy. The second step is based on the need to reduce the total number of cells and increase the accuracy in the whole area. So we only considered the sixth configuration, taking into account the field symmetry and the uniform hexahedral mesh tighter than the previous full configuration. Therefore, we adopted the grid of one sixth of the configuration, after many grid independence studies. The following Fig. 2 shows the meshed domain for both methods, and the boundary conditions are showed in Table II.

TABLE II  
 BOUNDARY CONDITIONS

Area	Boundary Conditions
Tank Walls	Wall
Turbine (Mixer+ Shaft)	Wall
Area around the Mixer	Moving Reference Frame (N=250 rpm)
Top of the Tank	Pressure Outlet ( $P^*=P_{\text{atm}}$ )

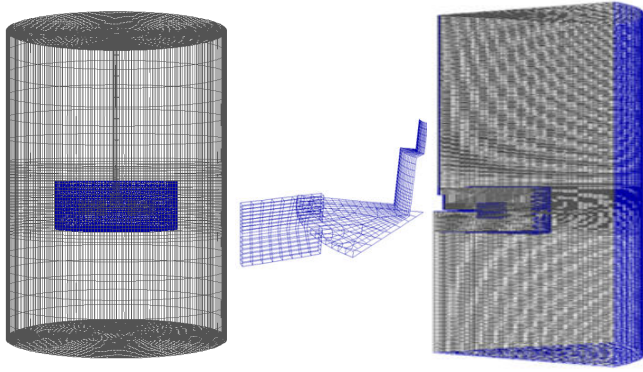


Fig. 2 Mesh of the studied field

### C. Governing Equations

In order to study the flow in our configuration and the various thermodynamic quantities characterizing it, we used a simulation model and the Euler-Euler multiphase. Unlike other models, the Euler model solves equations of transport and continuity for each phase. The coupling is then achieved through pressure and heat transfer coefficients between phases. In our case, a three-dimensional simulation was performed for an air-water multiphase system. The model MRF (Moving Reference Frame) was used to simulate the different interactions between the rotating turbine and the tank and its walls. The turbulence generated by the turbine is modeled using the turbulence model k-ε standard. This model is suitable for flows with fully developed turbulence (high Reynolds number). The details of the turbulence model, as well as those of the MRF model, and the equations governing these models will be discussed.

#### 1. Experimental Measurement of Fluid Viscosity

Measuring the viscosity of a fluid is a critical step in the simulation because it depends on the nature of the chosen fluid and the tool used to take measurements. In this section, we present our used fluid and the viscosity measurements. In our study, we have in our tank 27 liters of water. We will vary the viscosity by adding 250g of CMC in the water for the first case, 300g of CMC in the second case and 450g for the third case. We will have three solutions with a percentage by mass, respectively 0.9% CMC, 1.1% CMC and 1.7% CMC. The viscosity of non-Newtonian fluids is measured using a rheometer. We finally obtained the viscosity, the density and the Reynolds number of every studied fluid, which are summarized in Table III.

TABLE III  
 CHARACTERISTICS OF STUDIED FLUIDS

CMC Concentration (%)	$\mu$ (CPS) (1 Cps = $10^{-3}$ Pa.s)	$\rho$ (kg/m <sup>3</sup> )	Re
0	1.002	998.2	$6.4 \cdot 10^4$
0.9	16	1007.5	$4.10^3$
1.1	22	1009.3	$3.10^3$
1.7	32	1014.9	$2.10^3$

### 2. Conservation Equations:

The governing equations for an incompressible fluid can be written as:

$$\frac{\partial \rho}{\partial t} + \frac{\partial}{\partial x_i}(\rho u_i) = 0 \quad (1)$$

$$\frac{\partial}{\partial t}(\rho u_i) + \frac{\partial}{\partial x_j}(\rho u_i u_j) = -\frac{\partial P}{\partial x_i}(\rho u_i) + \frac{\partial}{\partial x_j} \left[ \mu \left( \frac{\partial u_i}{\partial x_j} + \frac{\partial u_j}{\partial x_i} \right) \right] + \frac{\partial}{\partial x_j}(-\overline{\rho u_i u_j}) \quad (2)$$

where the velocity components are divided into the mean  $\overline{u_i}$  and the fluctuating  $u'_i$  velocities. These two components are related to each other by the following equation:

$$u_i = \overline{u_i} + u'_i \quad (3)$$

Equations (1) and (2) are called Reynolds-Averaged Navier-Stokes (RANS) equations. The Reynolds stress term  $R_{ij} = \overline{\rho u'_i u'_j}$  represents the effects of turbulence and must be modeled to fully characterize (2).

### 3. MRF Model:

The computational domain for the CFD problem was defined with respect to the rotating frame so that an arbitrary point in the CFD domain is located by a position vector  $\vec{r}$  from the origin of the rotating frame. The fluid velocities can be transformed from the stationary frame to the rotating frame using the following relation:

$$\vec{v}_r = \vec{v} - \vec{u}_r \quad (4)$$

where

$$\vec{u}_r = \vec{\Omega} \times \vec{r} \quad (5)$$

In these equations  $\vec{u}_r$  is the “whirl” velocity (the velocity due to the moving frame),  $\vec{v}_r$  is the relative velocity (velocity viewed from the rotating frame), and  $\vec{v}$  is the absolute velocity (velocity viewed from the stationary frame). When the equations of motion are solved in the rotating reference frame, the acceleration of the fluid is augmented by additional terms that appear in the momentum equations. Moreover, the equations can be formulated in two different ways: Expressing the momentum equations using the relative velocities as dependent variables (known as the relative velocity formulation), or expressing the momentum equations using the absolute velocities as dependent variables in the momentum equations (known as the absolute velocity formulation).

#### 4. The Standard k-ε Model:

The standard k-ε model is a semi-empirical model based on model transport equations for the turbulence kinetic energy (k) and its dissipation rate (ε). The model transport equation for k is derived from the exact equation, while the model transport equation for ε was obtained using physical reasoning and bears little resemblance to its mathematically exact counterpart. The turbulence kinetic energy, k, and its rate of dissipation, ε, are obtained from the following transport equations:

$$\frac{\partial(\rho k)}{\partial t} + \frac{\partial(\rho k \bar{U}_i)}{\partial x_i} = \frac{\partial}{\partial x_j} \left[ \left( \mu + \frac{\mu_t}{\sigma_k} \right) \frac{\partial k}{\partial x_j} \right] + G_k + G_b - (\rho \varepsilon + Y_M) \quad (6)$$

and

$$\frac{\partial(\rho \varepsilon)}{\partial t} + \frac{\partial(\rho \varepsilon \bar{U}_i)}{\partial x_i} = \frac{\partial}{\partial x_j} \left[ \left( \mu + \frac{\mu_t}{\sigma_\varepsilon} \right) \frac{\partial \varepsilon}{\partial x_j} \right] + C_{1\varepsilon} \frac{\varepsilon}{k} (G_k + C_{3\varepsilon} G_b) - C_{2\varepsilon} \rho \frac{\varepsilon^2}{k} \quad (7)$$

In these equations,  $G_k$  represents the generation of turbulence kinetic energy due to the mean velocity gradients,  $G_b$  is the generation of turbulence kinetic energy due to buoyancy,  $Y_M$  represents the contribution of the fluctuating dilatation in compressible turbulence to the overall dissipation rate,  $C_{1\varepsilon}$ ,  $C_{2\varepsilon}$ , and  $C_{3\varepsilon}$  are constants,  $\sigma_k$  and  $\sigma_\varepsilon$  are the turbulent Prandtl numbers for k and ε, respectively, and  $S_k$  and  $S_\varepsilon$  are user-defined source terms.

### III. NUMERICAL RESULTS AND DISCUSSIONS

To study the viscosity effect in a stirred tank with a Rushton turbine, we will compare the numerical results from the calculation code Fluent of four solutions of different viscosities. When using only water, we are in a full turbulent regime, while for CMC solutions we are in transient regime. In this section we will study the different aspects and phenomena in a stirred tank with a Rushton turbine equipped with six blades, immersed at 7cm of the vessel free surface. Simulations are based on the assumptions chosen previously, with different viscosities of the fluid adopted. As a first step of this work, we focused on the volume fraction contours for the four studied cases, shown in Fig. 3.

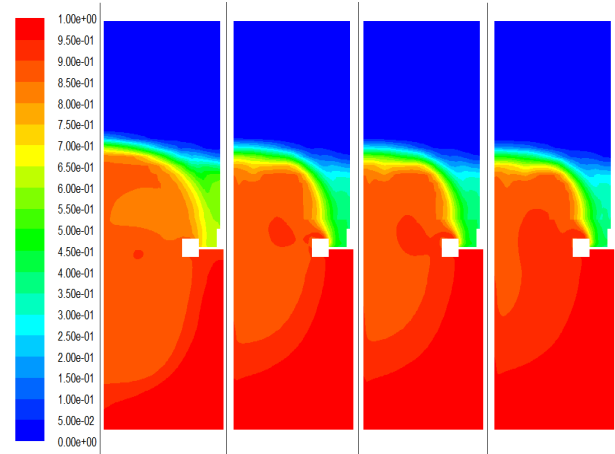


Fig. 3 Contours of the distribution of the volume fraction of phases in water containing a) 0% CMC, b) 0.9% CMC, c) 1.1% CMC and d) 1.7% CMC

We notice that the mixing phenomenon is more efficient for the smaller viscosity, i.e. the water case, with a less pronounced vortex. This is due to the resistance forces which increase with the increase of the fluid viscosity, so the mixing of air into the fluid is easier with a less viscous fluid. For the same reason, we have a stagnant area below the turbine which increase with viscosity, and this can also be explained by the turbine position which suits better for surface aeration, and provides a good mixing but not a perfect one. To better understand why the volume fraction contours are the way they are, we are now interested by the mean velocity vectors of various CMC concentrations in the mid plane with the rotational speed of 250 rpm shown in Fig. 4.

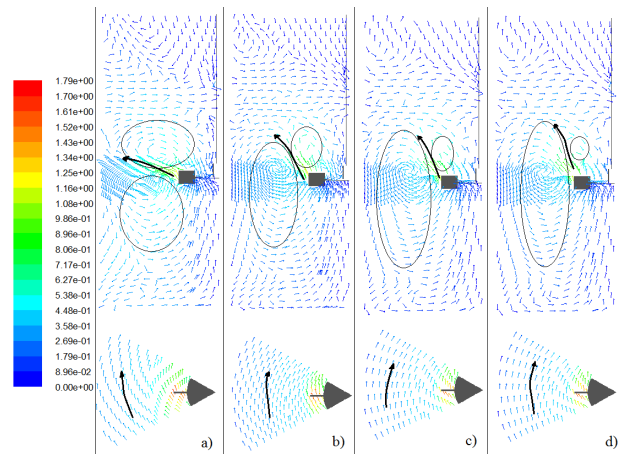


Fig. 4 Distribution of velocity vectors (m / s) for water containing a) 0% CMC, b) 0.9% CMC, c) 1.1% CMC and d) 1.7% CMC

We notice that the swirls are becoming smaller and weaker with the viscosity increasing. So they cannot reach the top and the bottom of the tank and secondary flow appears there and forms small swirls. The size of those swirls becomes smaller with the increase of the fluid viscosity and disappears finally, which confirm the fact that the decrease of viscosity led to a

better mixing. In fact, the fluid is mixed above and below the turbine blades for the case of water containing 0% of CMC, which is explained by the smaller frictional forces and resistance forces, and when the viscosity increases we see that the upper swirl size decreases and the lower swirl size increases. On the other hand, the jet delivered by the blade of the turbine is particularly directed to the top of the tank as the viscosity is higher. In the plane  $z = 0.20\text{m}$  we note that the velocity vectors, as a result of the increase in viscosity, is less directed to the vessel wall and define parallel and concentric streamlines. This is due to the fact that for larger values of viscosity, the flow generated by the turbine is transient and not turbulent as it is the case for the water containing 0% of CMC. As a confirmation to our deductions, we see in Fig. 5 the global velocity of the flow, which is less intense in the entire tank for higher values of viscosity. The maximum velocity also decreased around the blades as a result of the increase in the shear stress due to the increase of viscosity. The discharge of the turbine is moved up the tank for the highest values of viscosity. The shear rate is defined by the following equation:  $\tau = \mu \dot{\gamma}$  [Pa]. In our case  $\dot{\gamma} = 4.16 \text{ s}^{-1}$ , we will then have the values of shear rate of the other studied viscous fluids given in Table IV.

TABLE IV  
SHEAR RATE FOR DIFFERENT VISCOSITIES

CMC (%)	$\tau$ [mPa]
0	4.16
0.9	66.56
1.1	91.52
1.7	133.12

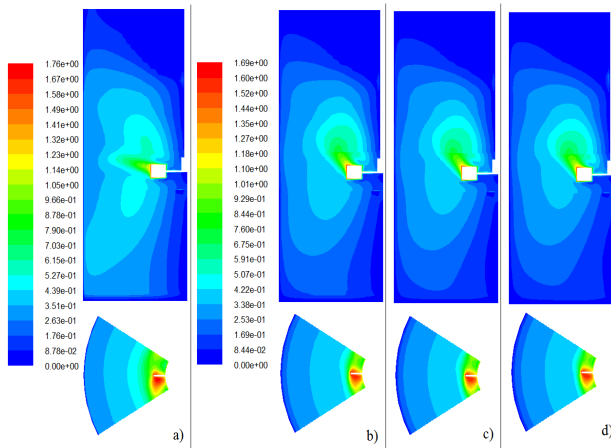


Fig. 5 Contours of the velocity magnitude of the flow (m / s) of water containing a) 0% CMC, b) 0.9% CMC, c) 1.1% CMC and d) 1.7% CMC

Now we will discuss the flow field behavior, with the radial, axial and tangential velocity profiles and contours, for the four studied case. The Rushton turbine is a radial flow impeller, so it is important to focus on radial profiles of the global velocity. Fig. 6 shows the radial profiles of the global velocity in the horizontal plane located at the level of the blade ( $z = 0.20\text{m}$ )

and the horizontal planes  $z = 0.185\text{m}$  and  $z = 0.215\text{m}$  located just below and just above the blade.

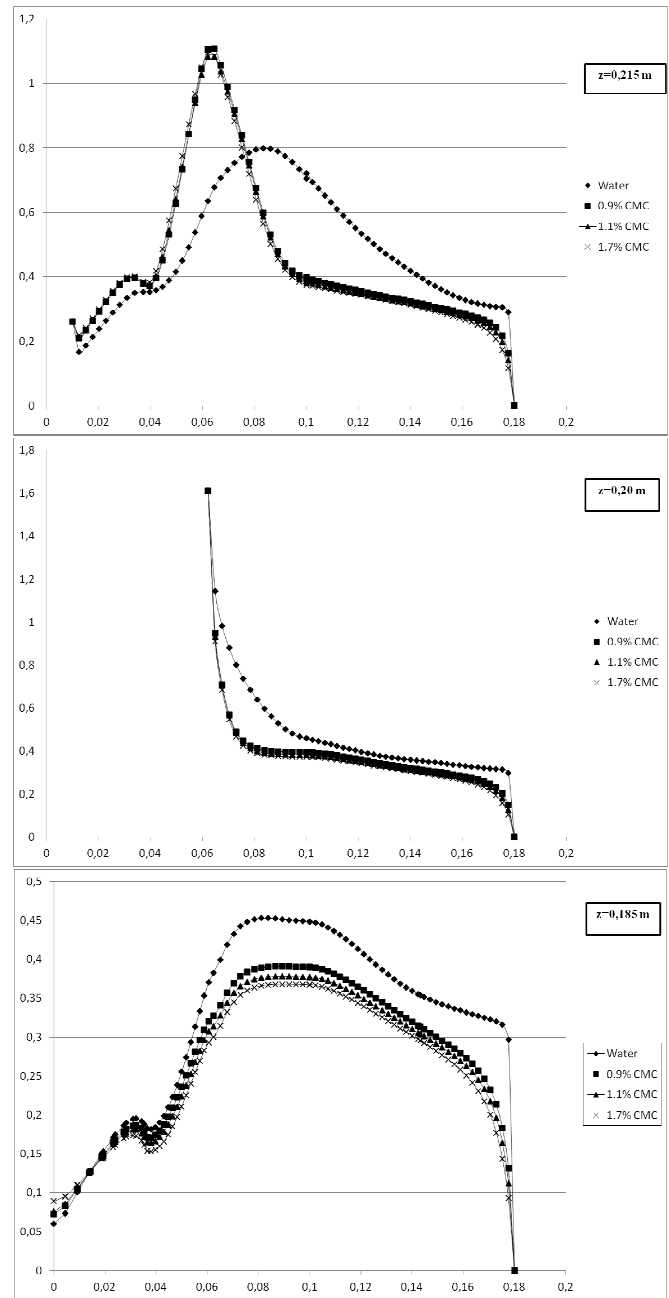


Fig. 6 Radial profiles of the velocity magnitude (m / s)

These planes were chosen because they better describe the flow field near the blades, which is the better mixing zone. At the blade level, the fluid leaves the latter with a velocity equal to  $U_{tip}$  and decreases rapidly. For water, the decrease gradient in speed is smaller compared to the other three cases. The profiles of the global velocity of CMC are all confounded above the blade and on the level of the blade. For the radial profile of the global velocity at the plane  $z = 0.215\text{m}$ , the speed is maximum for the radial position  $r = 0.08\text{m}$  in the case of water, while for the various solutions of CMC, it reaches its

maximum for the radial position  $r=0.062\text{m}$  which corresponds to the tip of the blade with a value greater than that achieved by water alone. This is due to the inclination of the jet delivered by the turbine blades up. Note that the velocity profiles for different CMC solutions are superposed and we do not really see the difference between a viscosity of 16Cps and a viscosity of 32Cps above the turbine disk. Just below the turbine disk, we can see a difference in the speed profile for the different viscosities. The speed is much lower when the viscosity increases. This difference is due to the fact that this zone is almost stagnant, so any variation of the radial speed is detected, as it is the case for the viscosity variation. To better understand the behavior of the radial Rushton turbine, it is now interesting to focus on the distribution of the radial velocity, shown in Fig. 7.

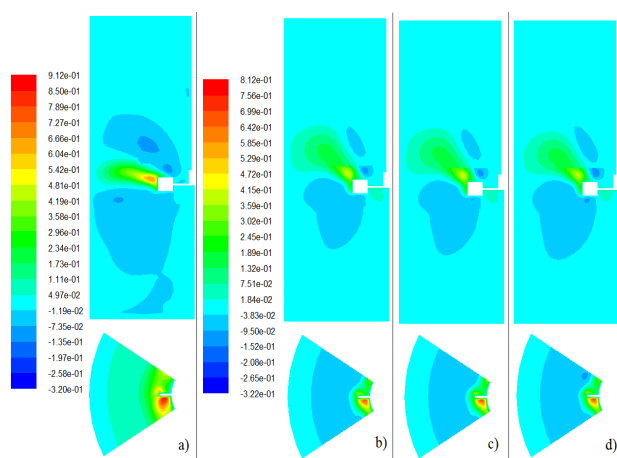


Fig. 7 Contours of the radial velocity (m / s) for water containing a) 0% CMC, b) 0.9% CMC, c) 1.1% CMC and d) 1.7% CMC

The discharge moved upwards loses its radial intensity as it is the case for the decrease in the radial velocity across the tank with the increasing viscosity. There is less reverse circulation in the recirculation loops and the wake driven by the turbine blades is less important when the viscosity increases. In the mid plane and just below the blade we noted that negative velocities occur in the case of CMC solutions. This creates a reverse flow mainly due to jet upward; we can see the effect of recirculation loops top and bottom. It is also interesting to consider the axial velocity of the flow in the stirred tank. The radial profiles of axial velocity in Fig. 8 show that the axial velocity corresponding to different values of the viscosity does not differ from each other, and as the radial velocity we also see that the case using only water have a greater axial velocity for the same radial position. This is due to the shear stress forces applied on the fluid, and which became more important as the fluid viscosity increase. There is also a difference in axial velocity just below the disc of the turbine where its value for 1.7% CMC is equal to twice that noted for water alone. This is explained by the fact that the adhesion of the fluid with the turbine disk is more important with a high viscosity fluid.

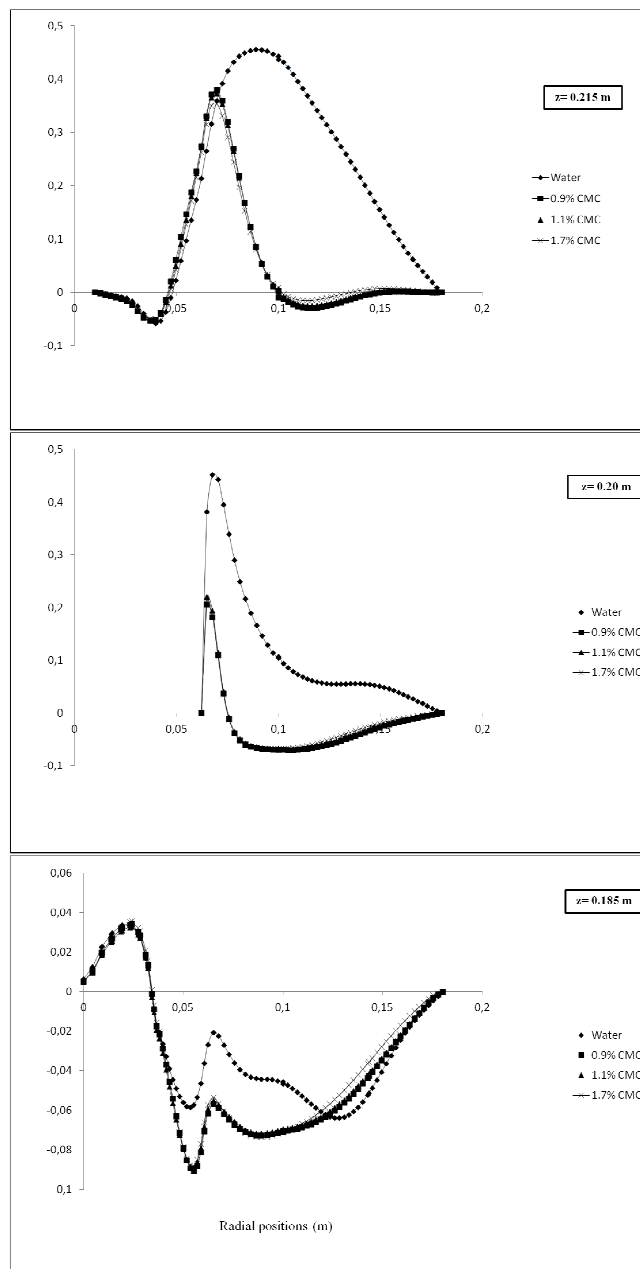


Fig. 8 Radial profiles of axial velocity (m / s)

We conclude that the viscosity change affects mainly the radial component and axial component of velocity. The fluid rheological behavior significantly changes the appearance of the velocity profiles and of the fluid flow. Indeed, water, a Newtonian fluid, creates a radial flow when agitated by a Rushton turbine, while the flow generated by the same type of turbine turns to an axial flow for a non-Newtonian fluid and keeps similar values when varying viscosity. So depending on our needs, we can create an axial flow behavior or a radial one, with varying the viscosity of our fluid. But the mixing process is better with a smaller viscosity, and we can improve this mixing with changing the turbine position by changing the turbine clearance.

We now focus on the viscosity effect on the turbulence

field, in the same median planes. In Fig. 9, we see the distribution of turbulent kinetic energy  $k$  for different viscosities. We notice that the turbulent kinetic energy " $k$ " is more important in zones of strong turbulence, which is in the discharge zone of the turbine. Away from the mixer, it gradually decreases to finally vanish in the vicinity of the side wall and the bottom of the tank, where no strong shear stress are noted. For the case of water containing 0% of CMC, we have a strong turbulent kinetic energy between two consecutive blades of the turbine, which is due to the low adhesion of the fluid with the turbine disk which consequently create an important turbulence in the vicinity of turbine blades. For the case of CMC solutions, this rate change, and there are energy values greater all around the blade and part of that energy follows the direction of the jet delivered by the turbine.

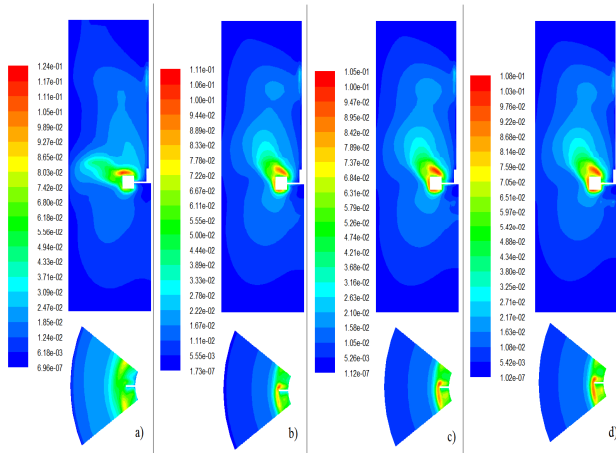


Fig. 9 Contours of turbulent kinetic energy  $k$  ( $m^2/s^2$ ) for water containing a) 0% CMC, b) 0.9% CMC, c) 1.1% CMC and d) 1.7% CMC

The maximum values of  $k$  are even lower than the viscosity is high. It is also accurate to note that for the cases with a percentage of CMC, the flow regime is transient, so the turbulence decreases with the increase of viscosity, which explain the contours of the turbulent kinetic energy  $k$  obtained. This is consolidated by the profiles of the turbulent kinetic energy, as we can see in Fig. 10. We see here, that above and below the turbine, the turbulent kinetic energy of water with 0% CMC is more important than the other three viscous fluids which are confounded for the three positions of study.

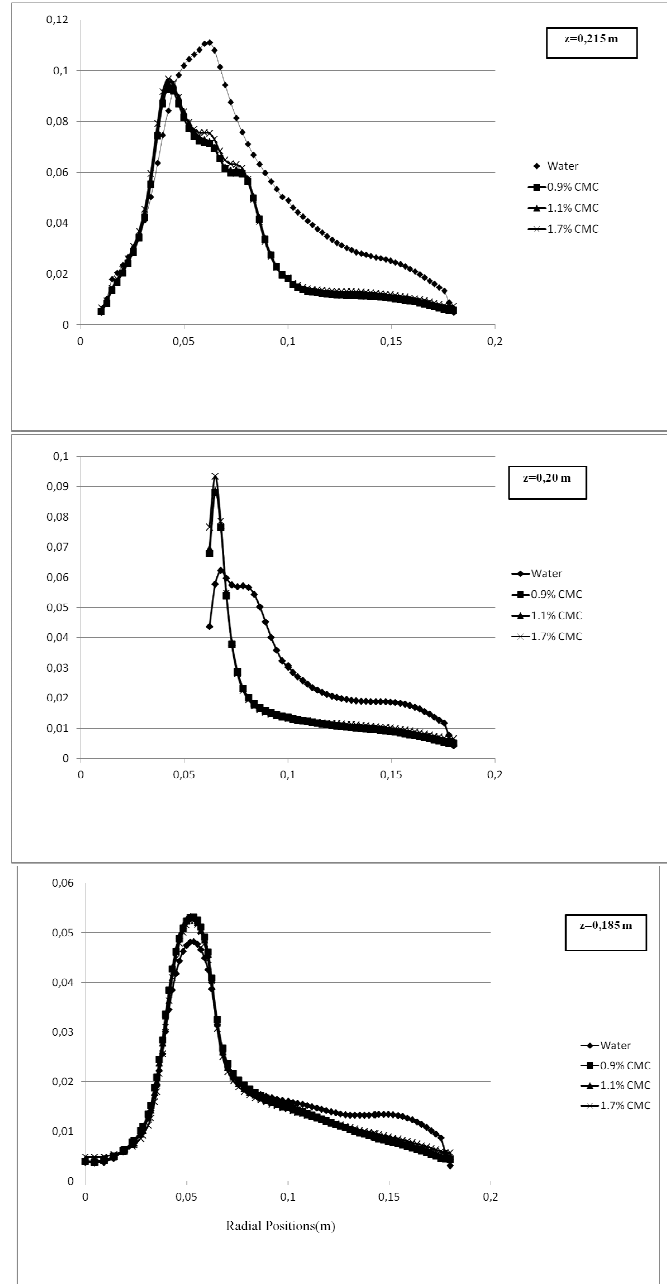


Fig. 10 Radial profiles of the turbulent kinetic energy  $k$  ( $m^2 / s^2$ )

Again here, we notice that this turbulent parameter have the same behavior qualitatively for the four fluids, just below the blades, which is explained by the stagnant zone present under the turbine. At the level of the blade, the turbulence is more important for the water with 0% CMC, and this is due to the viscosity of the fluid allowing a better mixing, so a more turbulent fluid, with an important gap on the tip of the blade. Note that the difference between the curves in the case of different concentrations of CMC is low, and at the plane  $z = 0.215m$  we see that the turbulent kinetic energy of viscous fluids is lower than the water turbulent kinetic energy, and we note again that it is much higher when the fluid viscosity increase which can be explained by the complex rheological

behavior of viscoelastic fluid. To better understand the turbulent behavior of our flow field, with the viscosity variation, we give in Fig. 11 the contours of turbulence intensity for the four studied cases.

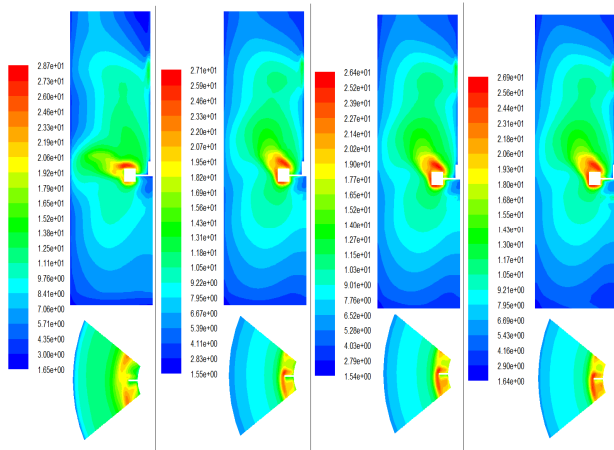


Fig. 11 Contours of turbulent intensity (%) for water containing a) 0% CMC, b) 0.9% CMC, c) 1.1% CMC and d) 1.7% CMC

It shows that the turbulence is less intense by increasing the viscosity. The appearance of the radial contours of the turbulence intensity is similar to that of the turbulent kinetic energy, due to correlations of proportionality between  $I$  and  $k$ . Below the blade, we see that the turbulence intensity for different viscosities remains unchanged while at the level of the blade and above the blade, the turbulence is more intense for the higher values of viscosity then it decreases suddenly to become less than the water turbulence in the rest of the tank. These contours confirm our previous interpretations: the more the fluid is viscous, less is the turbulence. This is due to the fact that for viscous fluids containing CMC, the flow regime is transient and the operation of mixing is more difficult and less perfect.

#### IV. CONCLUSION

The purpose of this work was to bring out the effect of fluid viscosity on the hydrodynamic parameters of the flow. We saw in this work the conduct of a viscous fluid, its velocity, its radial behavior and its turbulent character. As results, we concluded that for a better mixing of our fluids, using only water is advised and we have then a turbulent radial flow. But if it is preferred to have an axial transient flow, we can increase the viscosity of the fluid using a given percentage of CMC, the process of mixing is then at first but the axial flow is favored. Changing the clearance of our turbine can ameliorate the mixing and the hydrodynamic behavior of our flow field.

#### NOMENCLATURE

C:	Clearance, m
$C_{\epsilon i}$	Empirical constants of the k- $\epsilon$ model
D:	Impeller's diameter, m
d:	Diameter of the turbine's disk, m

E:	Thickness of the turbine's disk, m
$e_p$ :	Thickness of the blade, m
$G_k$ :	The generation of turbulence kinetic energy due to the mean velocity gradients
$G_b$ :	The generation of turbulence kinetic energy due to buoyancy
H:	Tank height, m
h:	Liquid height, m
k:	Turbulent kinetic energy, $m^2s^{-2}$
$l_p$ :	Blade width, m
$L_p$ :	Blade length, m
N:	Impeller rotation speed, rpm
$N_p$ :	Power number
$N_Q$ :	Pumping Number
$\vec{r}$ :	Position vector in the rotating sub domain
s:	Impeller submersion, m
t:	Time, s
T:	Tank diameter, m
$U_i$ :	i component of the instantaneous velocity vector, m/s
$\vec{u}_r$ :	Relative velocity vector
$\vec{u}$ :	Absolute velocity vector
$\vec{x}$ :	Absolute position in Cartesian coordinates
$\vec{x}_0$ :	Origin of the axis of rotation of the rotating field
z:	Axial position, m

#### Greek Symbols

$\rho$ :	Fluid density, $kg/m^3$
$\mu$ :	Fluid dynamic viscosity, Pa.s
$\mu_t$ :	Turbulent viscosity, Pa.s
$\epsilon$ :	Turbulent energy dissipated per unit mass, $m^2s^{-3}$
$\sigma_k, \sigma_\epsilon$ :	Empirical constants of the k- $\epsilon$ model
$\gamma_M$ :	The contribution of the fluctuating dilatation in compressible turbulence
$\beta$ :	Coefficient of thermal expansion
$\vec{\Omega}$ :	Angular velocity vector

#### REFERENCES

- [1] C. Gómez, C. P. J. Benington, and F. Taghipour. Investigation of the Flow Field in a Rectangular Vessel Equipped With a Side-Entering Agitator. *J. Fluids Eng.*, 2010. 132, 051106.
- [2] Si Y. Lee and Richard A. Dimenna. Applications of CFD Method to Gas Mixing Analysis in a Large-Scaled Tank. *ASME Conf. Proc.*, 2007. FEDSM2007.
- [3] Robert A. Leishear, Si Y. Lee, Mark D. Fowley, Michael R. Poirier, and Timothy J. Steeper. Comparison of Experiments to Computational Fluid Dynamics Models for Mixing Using Dual Opposing Jets in Tanks With and Without Internal Obstructions. *J. Fluids Eng.*, 2012. 134, 111102.
- [4] Paul A. Gillis, Gerrit Hommersom, and Matthias Schäfer. A Comparison of Several CFD Approaches for Predicting Gas-Liquid Contacting in a Cylindrical Tank Agitated With a Single Rushton Turbine. *ASME Conf. Proc.*, 2002. PVP2002.
- [5] Ranade, V.V.. An efficient computational model for simulating flow in stirred vessels: case of Rushton turbine. *Chem Eng Sci.*, 1997. Vol. 52, 24, 4473–4484.
- [6] NG, K. et al. Assessment of sliding mesh CFD predictions and LDA measurements of the flow in a tank stirred by a Rushton impeller. *Transl Chem E.*, 1998. Vol. 76, partA, 737-747.
- [7] Kumaresan, T et al. Effect of impeller design on the flow pattern and mixing in stirred tanks. *Chem Eng Sci.*, 2006. 115.
- [8] Mavors, P.. Flow visualization in stirred vessels-A review of experimental techniques. *Transl ChemE.*, 2001. Vol. 79, part A, 113-127.

- [9] Zadghaffari, R. et al. Large Eddy Simulation of turbulent flow in a stirred tank driven by a Rushton turbine. *Computer & Fluids*, 2010. Volume 39, Issue 7, 1183–1190.
- [10] Lu, W. et Yang, B.. Effect of blade on the structure of the trailing vortex around Rushton turbine impellers. *Can. J. Chem. Eng.*, 1998. Vol. 76, 556–562.
- [11] Ochieng,A. et al. Mixing in a tank stirred by a rushton turbine at a low clearance. *Chem. Eng. Process*, 2008. Vol. 47, 842-851.
- [12] Brucato, A et al. Numerical prediction of flow fields in baffled stirred vessels: A comparison of alternative modeling approaches. *Chem Eng Sci*, , 1998. Vol. 53, 21.
- [13] NG, K. et Yianneskis, M.. Observations on the distribution of energy dissipation in stirred vessels. *Trans I ChemE.*, 2000. Vol. 78, part A, 334-341.
- [14] Mavros, P et al. Determination of flow fields in agitated vessels by Laser-Doppler Velocimetry: Use and interpretation of RMS velocities. *Trans IChemE.*, 1998. Vol. 76, part A, 223-233.
- [15] Yundong, W. et al. PIV measurements and CFD simulation of viscous fluid flow in a stirred tank agitated by a Rushton turbine. Melbourne, Australia: CSIRO, Fifth International Conference on CFD in the Process Industries, 2006.
- [16] Triveni, B. et al. Mixing studies of non newtonian fluids in an anchor agitated vessel. *Chem. Eng. Res. Des.*, 2010. Vol. 88, 809-818.